Spatial segregation and aging of metabolic processes underlie phenotypic heterogeneity in mycobacteria

Authors: Celena M. Gwin[a,*], Kuldeepkumar R. Gupta[a,*], Yao Lu[a], Lin Shao[a], E. Hesper Rego[a,1]

Affiliations

[a] Department of Microbial Pathogenesis, Yale University School of Medicine, New Haven, CT 06519

* equal contribution

[1]To whom correspondence should be addressed: hesper.rego@yale.edu

Individual cells within clonal populations of mycobacteria vary in size, growth rate, and antibiotic susceptibility. Heterogeneity is, in part, determined by LamA, a protein found exclusively in mycobacteria. LamA localizes to sites of new cell wall synthesis where it recruits proteins important for polar growth and establishing asymmetry. Here, we report that in addition to this function, LamA interacts with complexes involved in oxidative phosphorylation (OXPHOS) at a subcellular location distinct from cell wall synthesis. Importantly, heterogeneity depends on a unique extension of the mycobacterial ATP synthase, and LamA mediates the coupling between ATP production and cell growth in single cells. Strikingly, as single cells age, concentrations of proteins important for oxidative phosphorylation become less abundant, and older cells rely less on oxidative phosphorylation for growth. Together, our data reveal that central metabolism is spatially organized within a single mycobacterium and varies within a genetically identical population of mycobacteria. Designing therapeutic regimens to account for this heterogeneity may help to treat mycobacterial infections faster and more completely.

Introduction

For a bacterial infection to linger after antibiotic treatment, only a few bacteria need to remain. What is different about surviving bacteria, and how do these differences arise? Despite extensive research, no single model has emerged explaining this phenomenon, and it is likely that the answers to these questions will vary depending on the bacterial species. In the case of model bacteria, like *Escherichia coli*, much of the focus has been on stochastic mechanisms that underlie cells switching into rare drug-tolerant states (*1, 2*). However, stochasticity is just one way of generating diversity, and other mechanisms of heterogeneity are more deterministic in nature. For example, clonal populations of mycobacteria, a genus that includes the human pathogen *Mycobacterium tuberculosis*, exhibit more variability than model bacterial species (*3*). At least some of the heterogeneity is created every time a mycobacterium divides when it produces two cells with different sizes, growth rates, and susceptibilities to antibiotics (*4*). Importantly, heterogeneity is hard-coded in the genome, as deletion of a single gene unique to mycobacteria – *lamA* – collapses morphological heterogeneity and leads to fast and uniform killing by several antibiotics (*5*). LamA localizes to sites of new cell wall synthesis and recruits proteins important for polar growth (*6*). However, many bacterial species divide asymmetrically but do not exhibit as much heterogeneity as mycobacteria, suggesting that asymmetric division is only one factor responsible for creating a heterogeneous population (*7*). Here, we sought to understand the mechanism by which LamA creates heterogeneity in growth.

Results

A conserved tyrosine regulates the localization and function of LamA

The predicted structure of LamA includes two regions of high disorder separated by a single transmembrane domain (**Fig. 1A**). The carboxy terminus of the protein is predicted to encode an MmpS domain. Proteins with these domains are often encoded by operons that include *mmpL* genes, but LamA's operon partner is a gene of unknown function. The amino terminus of LamA

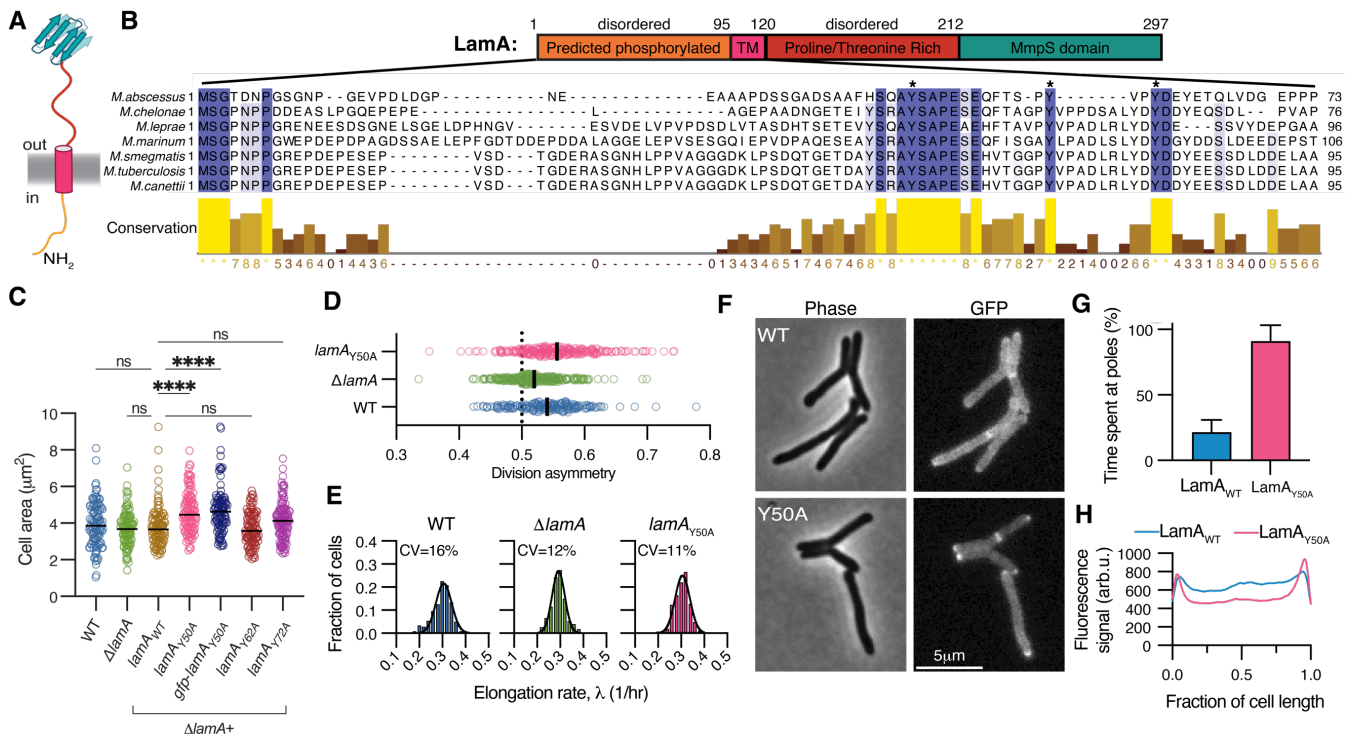

Figure 1. A conserved phosphorylated tyrosine is important for LamA function and localization. **(A)** Schematic of the predicted structure of LamA. **(B)** A multiple sequence alignment of the N-terminal sequence of LamA. Stars indicate residues mutated in panel C. **(C)** Cell size of WT, Δ*lamA*, or cells expressing the indicated *lamA* allele in Δ*lamA*. (dark black lines indicate medians; n=100-125 cells for all strains; ****p<0.0001 by one-way ANOVA comparing means to $lamA_{WT}$ corrected for multiple comparisons). **(D)** Asymmetry in the daughter cell size at the time of division, measured by the old pole daughter as a fraction of the total size of both daughters. The dotted line marks symmetric division. (n=195, 236, 223 daughter cell pairs for WT, Δ*lamA*, and $lamA_{Y50A}$, respectively). **(E)** The elongation rate, λ, of the indicated strains. (CV = coefficient of variation, n=239, 226, 267 single cells for WT, Δ*lamA*, and $lamA_{Y50A}$, respectively). **(F)** Phase contrast and fluorescence images of either msfGFP-LamA or msfGFP-$LamA_{Y50A}$ expressed in single copy from the native promoter. **(G)** Fractional dwell time of strains in panel F calculated by the amount of time a focus spent at the pole before dissipating, normalized to the total time of a fast-interval timelapse (n=15 cells for each strain). **(H)** Intensity profiles were measured across several cells, normalized to cell length, and averaged (n =140-165 cells for each strain). In panels D & E, $LamA_{Y50A}$ refers to the strain mutated on the chromosome in an otherwise wild type background. In all others, $lamA_{Y50A}$ is expressed in single copy in Δ*lamA*.

is highly acidic, with nearly 20% of the residues in this region being either aspartic or glutamic acid. Additionally, several whole-cell proteomic studies have mapped phosphorylation events at serine, threonine, and tyrosine residues in this region (*8-13*). We performed a multiple sequence alignment of LamA proteins found throughout the mycobacterial genus and observed that, despite the predicted disorder of this region, several tyrosine and serine residues were highly conserved (**Fig. 1B**). To test the function of these residues, we created phage-integrating plasmids carrying alanine mutations at each of these sites, transformed these into Δ*lamA M. smegmatis,* and

60 imaged the resulting strains by phase contrast microscopy. To quantify the morphology of single
61 cells, we trained the U-Net machine-learning software package to detect and segment single
62 mycobacterial cells by phase contrast (*14, 15*). Using this approach, we found that one mutant, a
63 tyrosine mutated to an alanine at position 50, resulted in cells that were slightly larger than the
64 other mutants and wild type (**Fig. 1C**). Increased cell size was due to an increase in cell length
65 rather than width (**Fig. S1**). Importantly, tyrosine 50 is found to be phosphorylated in several
66 whole-cell proteomic studies (*9-11*). To confirm that this mutation is important at the native locus,
67 we used marker-less single-strained recombineering (*16*) to recode this tyrosine to an alanine at
68 the native locus and performed timelapse microscopy. Compared to wild type cells, a
69 subpopulation of cells expressing $LamA_{Y50A}$ was indeed larger, driving the increased size of cells
70 across the population (**Fig. S2**). This also led to more heterogeneity in cell size at the time of
71 division; however, it did not change the asymmetry at division (**Fig. 1D, Fig S2**). Both phenotypes
72 suggested that $LamA_{Y50A}$ functions similarly to $LamA_{WT}$ or may be a gain-of-function mutant.
73 However, this mutant was deficient in other functions performed by LamA. Specifically,
74 LamA also affects the heterogeneity in single-cell growth rate. Biochemical fluctuations within
75 metabolic pathways result in individual cells growing at slightly different rates centered around a
76 population average (*17*). To compare growth rate distributions between strains, we relied on the
77 observation that single *M. smegmatis* cells grow exponentially and computed an average growth
78 rate, $\lambda = \ln(S_d/S_b)/\Delta T$, where S_d is the size of the cell at division, S_b is the size of the cell at birth,
79 and ΔT is the time between birth and division (*18*). Wild type *M. smegmatis* displayed 16%
80 variation in λ, in agreement with prior studies that computed λ by measuring length instead of
81 area (*18, 19*). In contrast, both Δ*lamA* and $LamA_{Y50A}$ cells were less variable than wild type (CV_λ
82 = 12% and 11%, respectively) (**Fig. 1E**). Computing growth by other metrics resulted in the same
83 conclusion (**Fig. S3A**). Importantly, expression of $LamA_{WT}$ from an integrative plasmid restored
84 heterogeneity in Δ*lamA* (**Fig. S3B**). Thus, LamA has at least two functions. One establishes

85 asymmetry in cell size at the time of division; the other is dependent on tyrosine 50 and mediates
86 heterogeneity in the growth rate of single cells.

87 To understand what was different about $LamA_{Y50A}$, we fused msfGFP to either the wild
88 type or mutant variant of LamA at their N-termini and expressed these from the native promoter
89 at a phage integration site in Δ*lamA*. We had previously determined that LamA localized to the
90 septum, but were unable to visualize membrane localization, possibly due to over-expression of
91 the fusion construct (*5*). By expressing msfGFP fusions at native levels, we observed that, in
92 addition to localizing to the septum, msfGFP-$LamA_{WT}$ also localizes along the sides and is
93 occasionally found at the poles (**Fig. 1E**). Timelapse imaging at 5-minute intervals confirmed that
94 msfGFP-$LamA_{WT}$ is highly dynamic between the pole and sides of the cell, at a timescale that is
95 too fast to represent new synthesis and maturation of the fluorescence protein fusion construct
96 (**Fig. 1F-H)**. We next localized msfGFP-$LamA_{Y50A}$ and found its localization to be much less
97 dynamic, with the protein primarily localized to the poles (**Fig. 1F-H**). Interestingly, the human
98 pathogen *M. tuberculosis* divides less asymmetrically than *M. smegmatis* but, like *M. smegmatis*,
99 exhibits a wide variation in single-cell growth rates (*20*). As we have connected LamA to both
100 asymmetric division and growth rate heterogeneity, we wondered if the *M. tuberculosis* LamA
101 variant localized differently than *M. smegmatis* LamA. Indeed, we find the *M. tuberculosis* variant
102 of LamA expressed in *M. smegmatis* is mainly found along the side walls, with less polar
103 localization than we observe with the *M. smegmatis* variant (**Fig. S4**).

104 Taken together, these data reveal that the functions of LamA are performed at different
105 subcellular sites and that LamA dynamically localizes between these sites, possibly in a
106 phosphorylation-dependent manner. Specifically, we find that a mutant of LamA that cannot be
107 phosphorylated at a conserved residue is locked at the poles and grows more uniformly. This
108 suggests that the mechanisms used to create heterogeneity in growth are performed along the
109 sides of the bacterium. Furthermore, these data suggest that LamA functions at the pole to

110 establish asymmetric polar growth. In fact, we have recently shown that LamA is important for
111 recruiting certain proteins to the poles, which are required to establish asymmetry (*6*).
112
113 **LamA precipitates with proteins involved in oxidative phosphorylation, which are excluded**
114 **from the poles and septa**
115 As LamA is performing different functions at distinct subcellular sites, we hypothesized
116 that it would interact with different proteins depending on its localization. To examine this, we
117 performed a series of immunoprecipitations to find potential protein-protein interaction partners.
118 We created a strain in which the sole copy of LamA was fused to the 3X-FLAG epitope. We fixed
119 these cells with a chemical crosslinker to capture potentially transient interactions, incubated
120 lysates with α-FLAG beads, and identified co-precipitating peptides by mass spectrometry.
121 Precipitated peptides largely fell into two categories of proteins – those associated with cell
122 elongation (MmpL3, PgfA, MurA, and PknA), and those associated with cellular respiration and
123 oxidative phosphorylation (components of the electron transport chain and ATP synthase
124 complex) (**Table S1**). To verify these results, we conducted a reciprocal co-immunoprecipitation
125 with AtpG, the gamma subunit of ATP synthase, since it was highly enriched in multiple biological
126 replicates. For this, we created strains expressing both AtpG-3XFLAG and LamA-strep and found
127 that we could precipitate LamA-strep with α-FLAG beads only when AtpG-3XFLAG was present
128 (**Fig. 2A**).
129 Perhaps shedding light on these interactions, the operon containing *lamA* is arranged in
130 the middle of two operons containing many of the genes that encode proteins in the cytochrome
131 III/IV supercomplex, which performs the last step in the electron transport chain (ETC). This
132 genomic synteny is conserved across mycobacterial species (**Fig. 2B,C**). To further investigate
133 the connection between LamA and the ETC, we tracked the localization of QcrB, a subunit of the
134 III/IV supercomplex, by making an in-frame fusion to msfGFP at the chromosomal locus. We also

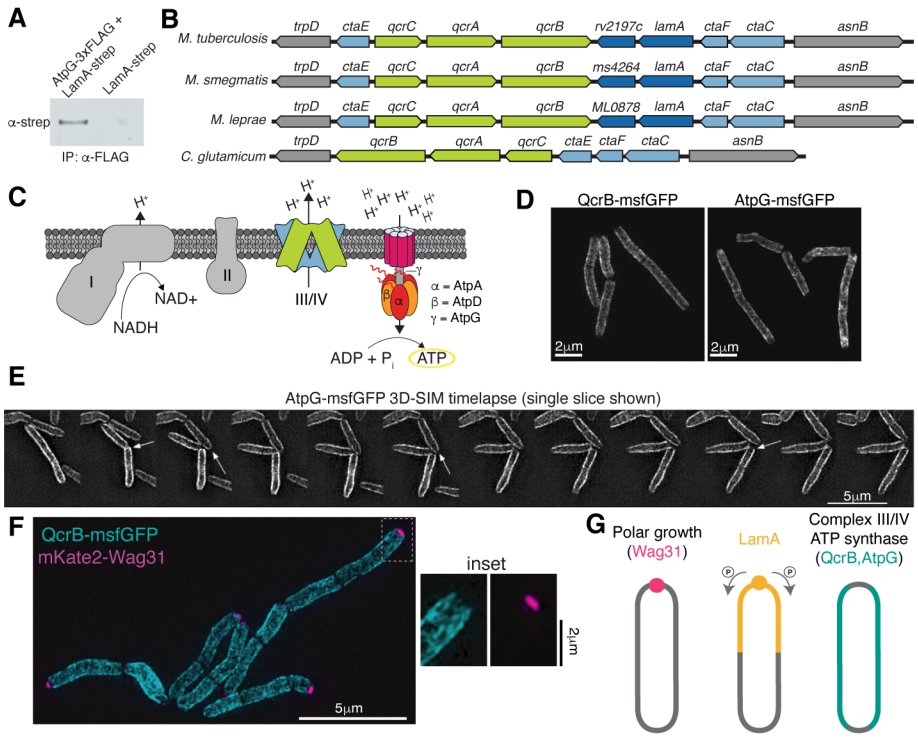

Figure 2. LamA interacts with proteins involved in OXPHOS, which are spatially separated from those used to grow the cell.
(A) Strains expressing the indicated epitope-tagged proteins were incubated with α-FLAG beads, and the precipitates were probed with an α-strep antibody via Western blot. **(B)** The genomic region surrounding *lamA* in the indicated organisms. **(C)** The proteins in the ETC that correspond to the genes in panel B. **(D)** Live cells expressing the indicated fusions were imaged by 3D-SIM. A maximum projection is shown. **(E)** Cells expressing AtpG-msfGFP were followed over time by 3D-SIM at 15-minute increments. At each time point single slices from the 3D stacks are shown. Arrows indicate AtpG dynamically infiltrating the tips of cells. **(F)** Cells expressing fusions to QcrB and Wag31 were imaged by live-cell 3D-SIM. A maximum projection is shown. **(G)** A model summarizing the localization of LamA and the complexes involved in polar growth and OXPHOS.

created fusions to AtpG and AtpA, the gamma and alpha subunits of the ATP synthase complex, respectively. As expected, by conventional fluorescence microscopy, the proteins were localized to the plasma membrane (**Fig. S5A**). To visualize the localization of these proteins more closely, we loaded cells into a microfluidic device and performed live-cell three-dimensional structured-illumination microscopy (3D-SIM), a super-resolution technique. As SIM requires collecting several images to reconstruct one super-resolved image, we focused on AtpG and QcrB fusions because these were the brightest. We collected images at single time points and observed that

142 both proteins were excluded from the tips of the cells as well as the septa of dividing cells (**Fig.**
143 **2D**). By timelapse 3D-SIM at 15-minute increments, we occasionally saw AtpG-msfGFP infiltrate
144 the tip of the cell but primarily remain localized to the sides of the cell (**Fig. 2E**). To visualize the
145 localization in the context of proteins that direct polar growth, we created a strain that encoded
146 key polar growth scaffolding protein, Wag31, fused to mKate2 in the background of cells
147 expressing QcrB-msfGFP and performed two-color live-cell 3D-SIM (**Fig. 2F,G**). We observed
148 little to no colocalization between these two proteins, showing that the complexes that perform
149 the last steps of oxidative phosphorylation are spatially distinct from those involved in growing the
150 bacterium (**Fig. 2F, Fig. S5B)**. Moreover, as LamA is localized dynamically between the
151 poles/septa and sides, these data also suggest that the interaction between LamA and the
152 electron transport chain is transient and largely confined to the sides, rather than poles, of the
153 bacterium (**Fig. 2G**).
154
155 **LamA inhibits oxidative phosphorylation, and reliance on oxidative phosphorylation is**
156 **associated with uniformity.**
157 If LamA is working with the respiratory chain, we reasoned that changes to the membrane
158 potential and cellular ATP levels might reveal if it has a negative or positive regulatory role. We
159 measured membrane potential by quantifying the accumulation of a charged fluorescence
160 molecule, TMRM, by flow cytometry (*21, 22*). As a control, we treated cells with a known
161 protonophore, CCCP, at greater-than-MIC concentrations to depolarize the membrane and
162 observed the expected decrease in signal (**Fig. 3A**). Compared to wild type, Δ*lamA* was slightly
163 depolarized (**Fig. 3A**), supporting the idea that LamA is functioning with members of the electron
164 transport chain. Next, we measured ATP levels using a standard luminescence-based assay and
165 found that ATP levels were slightly higher in Δ*lamA* cells (**Fig. S6A**). Together, these data suggest
166 that LamA may be inhibiting the production of ATP via oxidative phosphorylation.

Oxidative phosphorylation is essential for mycobacteria, but mycobacteria can also produce ATP in other ways, like substrate-level phosphorylation when grown on sugars. We wondered how generalizable the connection between metabolism and heterogeneity was. Specifically, we asked if cells grown in conditions promoting the exclusive use of oxidative phosphorylation would phenocopy Δ*lamA*. To test this, we grew cells in defined minimal media and supplied succinate as the sole carbon source. Consistent with our hypothesis, wild type *M. smegmatis* grew uniformly in minimal succinate medium, and deletion of *lamA* had no additional effect on heterogeneity (**Fig. 3B**). *M. smegmatis* cells cultured in acetate also grow uniformly (*19*), suggesting this phenomenon is not specific to succinate-grown cells. To understand if this was also true in slow-growing mycobacteria, we followed single *Mycobacterium bovis* BCG cells for approximately four doublings (~4 days) in both our normal medium (7H9) and minimal medium supplied with succinate. Consistent with our findings in *M. smegmatis*, BCG cells cultured in 7H9 grew more

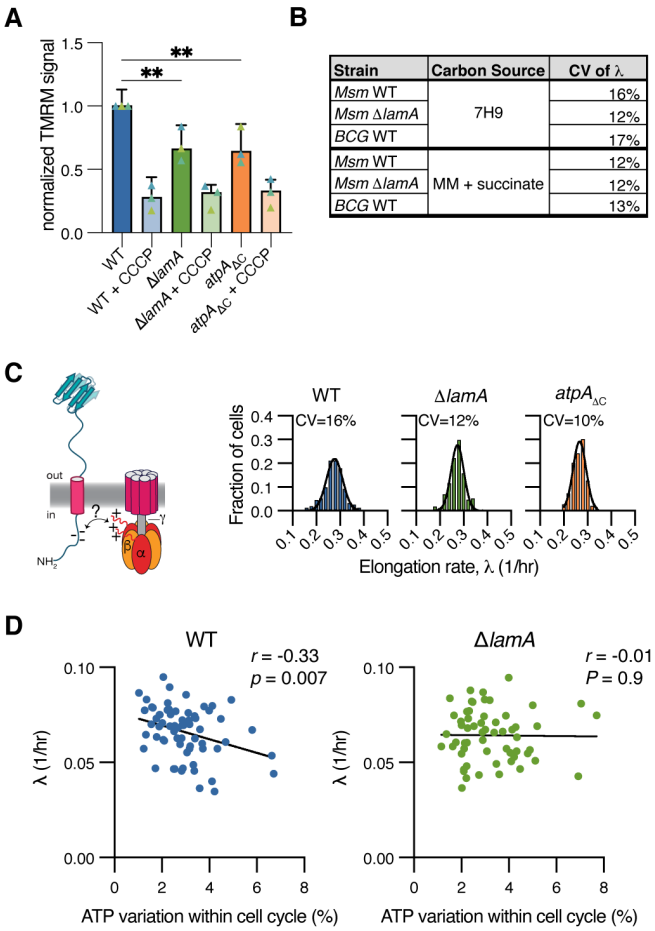

Strain	Carbon Source	CV of λ
Msm WT	7H9	16%
Msm Δ*lamA*		12%
BCG WT		17%
Msm WT	MM + succinate	12%
Msm Δ*lamA*		12%
BCG WT		13%

Figure 3. LamA-mediated heterogeneity is tightly linked to ATP production. (A) Accumulation of TMRM is measured by flow cytometry. As a control, cells were treated for 15 minutes with 500μM of CCCP. The bars represent the medians of three experiments (each with 3 biological replicates (triangles)) assayed on different days. Error bars are 95% confidence intervals. **p<0.002 by one-way ANOVA. **(B)** The indicated strains were grown in either 7H9 or minimal media (HdB for *Msm* or MMAT for *BCG*) supplied with succinate as the sole carbon source and imaged by phase contrast timelapse microscopy to compute λ for single cells. **(C)** Mycobacteria encode an unusual domain in the alpha subunit of the ATP synthase that prevents hydrolysis. We hypothesize that this positively charged extension interacts with the negatively charged cytoplasmic tail of LamA. Cells missing this extension were imaged over time to measure λ. (n = 152, 172, and 149 cells for WT, Δ*lamA,* and *atpA*Δ*C* cells, respectively). **(D)** WT or Δ*lamA* cells expressing the QUEEN-2m ATP biosensor were imaged over time, and the ratio of the two QUEEN excitation wavelengths was used to obtain relative ATP levels. For each cell, the variation within a cell cycle (as measured by the standard deviation of the QUEEN-2m signal divided by its mean) was compared to the exponential growth rate (n = 67 and 59 complete cell cycles for WT and Δ*lamA*, respectively; lines represent linear regressions; *r* is Pearson's correlation coefficient; and, *p* is the *p*-value).

193 heterogeneously than those fed only succinate (CV_{λ} = 17% and 13%, respectively) (**Fig. 3B**).
194 Together, these data show that cells undergoing more oxidative phosphorylation, either through
195 deletion of *lamA*, or through carbon source availability, grow more uniformly.
196
197 **An unusual extension on the ATP synthase alpha subunit mediates heterogeneity.**
198 We hypothesized that the interaction between LamA and OXPHOS proteins is important
199 for creating heterogeneity in the growth rate of single cells. The complexes that perform oxidative
200 phosphorylation in mycobacteria are comprised of highly conserved proteins, but there are
201 several unique characteristics specific to mycobacteria and related species (*23*). For instance, in
202 many organisms, ATP synthase can both synthesize and hydrolyze ATP depending on cellular
203 conditions. However, in some actinobacteria, including mycobacteria, the alpha subunit of ATP
204 synthase has a disordered extension (residues V519 – A548) that interacts with the gamma
205 subunit to prevent the enzyme from hydrolyzing ATP (*24*). The ATP synthase operon is duplicated
206 in *M. smegmatis (25)*; therefore, we created a strain in which we deleted the extension in both
207 copies of AtpA ($atpA_{\Delta C}$). Consistent with the known function of this extension to block ATP
208 hydrolysis, $atpA_{\Delta C}$ cells have slightly lower ATP levels (**Fig. S6B)**.
209 Because the extension on AtpA is highly positively charged, and the N-terminal extension
210 of LamA is negatively charged both by amino acid residues and by multiple phosphorylated
211 residues, we hypothesized that these two proteins might be interacting electrostatically (**Fig. 3C**).
212 To that end, we reasoned that if LamA interacts with this extension to inhibit ATP synthase, a
213 condition we have shown is associated with more heterogeneity, then we should expect that
214 $AtpA_{\Delta C}$ cells would phenocopy Δ*lamA* cells with regards to both membrane potential and single-
215 cell growth heterogeneity. To test membrane potential, we used the same TMRM assay as before
216 and found that the depolarization in $atpA_{\Delta C}$ cells was similar in magnitude and direction as that of
217 Δ*lamA* cells (**Fig. 3A**). Next, we analyzed single-cell growth by phase contrast timelapse
218 microscopy, and consistent with our hypothesis, $atpA_{\Delta C}$ cells exhibit less variability in growth than

219 wild type cells (**Fig. 3C)**, but not division asymmetry **(Fig. S7).** Further experiments will be needed
220 to determine if LamA and ATP synthase interact directly, a challenging directive as our data
221 suggests any interaction is likely transient. Nevertheless, we conclude that both LamA and an
222 actinobacteria-specific feature of the ATP synthase are needed to create phenotypic
223 heterogeneity within a genetically identical mycobacterial population.
224
225 **LamA mediates the coupling between ATP fluctuations and growth in single cells.**
226 Cellular ATP levels are often assumed to be uniformly distributed across a population and stable
227 over the course of a cell cycle. However, fluorescent biosensors that dynamically report on ATP
228 concentrations in single bacterial cells have revealed that ATP levels vary from cell to cell and
229 fluctuate dynamically within a cell cycle (*26, 27*). For single cells within a clonal population, large
230 ATP fluctuations during a cell cycle are associated with slower growth (*28*). While the biological
231 basis for this phenomenon remains unknown, it offers a potential explanation for phenotypic
232 heterogeneity in growth rate. Since we show that LamA is connected to ATP generation through
233 oxidative phosphorylation, we hypothesized that ATP fluctuations would be altered in Δ*lamA* cells.
234 To assay this, we expressed a codon-optimized version of the QUEEN-2m biosensor in *M.*
235 *smegmatis* cells with and without *lamA (26)*. ATP concentration within bacterial cells is linearly
236 proportional to the ratio of fluorescence excited at 405nm versus 488nm detected by the same
237 emission bandpass (*26*). Thus, we computed pixel-by-pixel ratios of the fluorescence values
238 collected at these wavelengths. As in *E. coli (26)*, single-cell measurements revealed a negative
239 correlation between the amplitude of fluctuation of QUEEN-2m signal (*i.e.* [ATP]) and growth rate
240 in wild type *M. smegmatis* cells. On average, Δ*lamA* cells displayed a similar magnitude of ATP
241 fluctuation, but these fluctuations were not correlated with growth rate (**Fig. 3D**). Together, these
242 data show that LamA mediates the coupling between ATP production and growth rate across a
243 clonal population of *M. smegmatis* cells.
244

Mycobacterial single-cell aging is associated with metabolic heterogeneity.

After division, rod-shaped cells inherit a new pole formed from the most recent division event and an old pole that was formed during a prior division event. For mycobacteria, this means that cells inherit growing poles of various ages (**Fig. 4A**). Cells with the oldest poles are born larger but grow more slowly and with more variability (*19, 29-31*). As we have connected growth variability to the production of ATP, we wondered how the abundance of OXPHOS components differed as single cells aged. By timelapse microscopy, we observed that the fluorescence intensity of QcrB-msfGFP (a proxy for the cellular concentration of QcrB) was inherited unevenly at division. On average, "old pole" cells inherited a lower concentration of QcrB than their "new

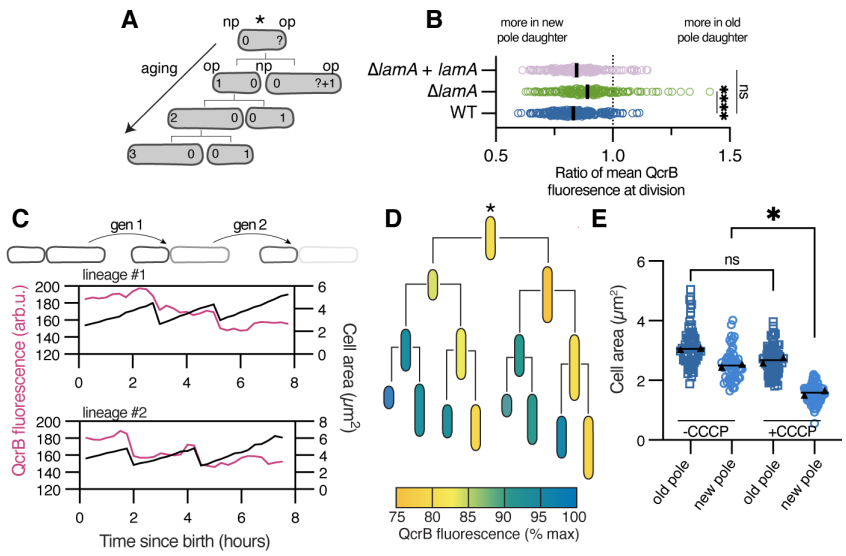

Figure 4. Metabolic aging in single mycobacterial cells.
(A) Schematic of aging cells and their associated pole ages. **(B)** QcrB-msfGFP fluorescence in the new pole daughter is compared to the fluorescence in the old pole daughter at the time of division in the indicated strains. The dotted line represents equal inheritance. **** $p<0.0005$ by one-way ANOVA. (n = 187, 191, and 159 sister pairs for WT, Δ*lamA*, Δ*lamA* +*lamA*, respectively). **(C)** QcrB-msfGFP fluorescence was followed over time in old pole daughters as they age. Two representative lineages are shown. **(D)** QcrB-msfGFP fluorescence over multiple generations, coloring corresponds to percent signal normalized to the maximum (n = 10 lineages). The initial mother cell is of unknown age as indicated by the * in panel A. **(E)** Cells grown in a microfluidic device and treated with 50μM CCCP. Size was measured pre- and post-treatment. (From left to right: n = 43, 40, 64, 47 over two different experiments, indicated by the triangles). $P<0.05$ by one-way ANOVA comparing the means of the triangles.

254 pole" siblings. This difference was reduced in Δ*lamA,* with a more uniform inheritance of subunits
255 between sisters (**Fig. 4A**).
256 We next asked how these differences propagated through the generations in a wild type
257 population. Thus, we identified the youngest cells in our timelapse data and followed them for at
258 least two generations. For many old pole daughters, we observed that fluorescence decreased at
259 time of division and declined steadily over multiple divisions (**Fig. 4C, 4D**). Analyzing multiple
260 lineages showed that QcrB concentration decreased in the old pole daughter cells by
261 approximately 25% after the third division (**Fig. S8A,B**). Reconstructing complete lineages
262 revealed that this phenomenon occurred to a greater or lesser degree depending on the identity
263 of the mother cell and was most pronounced in cells with the oldest mothers (**Fig. 4D**). We
264 repeated these measurements with cells expressing AtpG-msfGFP and observed similar trends
265 (**Fig. S8C,D**). Together, these data suggested that new pole progeny may be performing more
266 oxidative phosphorylation than older cells. To test this, we inhibited the proton motive force with
267 the protonophore CCCP and watched the response at the single-cell level. Consistent with our
268 hypothesis, the growth of new pole cells was affected by CCCP, while old pole cells were largely
269 unaffected (**Fig. 4E)**. These results phenocopy LamA overexpression (*5*), further supporting the
270 notion that LamA inhibits oxidative phosphorylation. Together, these data suggest a model
271 whereby mycobacteria aging at the single-cell level is associated with less reliance on oxidative
272 phosphorylation. Consequently, in an asynchronous population of mycobacterial cells, flux
273 through central metabolism varies from cell to cell.
274
275 **Conclusion**
276 Despite their small size, bacteria encode diverse mechanisms to spatially structure their internal
277 biochemical processes. For example, many bacteria rely on concentration gradients along their
278 long axis to spatially organize the macromolecular machines that perform division (*32-35*).
279 Additionally, at division, the concentration of secondary messengers like cyclic-di-GMP, can be

asymmetrically distributed, an event needed for the pathogenic lifecycle of *P. aeruginosa* *(36)*. Our work shows that central metabolic processes like those that produce energy can be subcellularly orchestrated in bacteria. Further work will be needed to understand the source of the connection between fluctuations in ATP levels and growth of single cells, which in mycobacteria is mediated by LamA. We speculate that the subcellular utilization of the proton motive force is an important component of this correlation. The proton motive force is a key resource for a bacterial cell – it powers the molecular machine needed to synthesize ATP and is used by numerous integral membrane proteins to transport various substrates, including molecules that make up the cell envelope, across the plasma membrane. In bacteria that grow by incorporating new envelope along their sides, complexes that use the proton motive force to grow and make ATP spatially intermingle. In contrast, we show that these two processes are spatially distinct in mycobacteria, with the proteins needed for oxidative phosphorylation found along the sides of the bacterium and certain pumps like MmpL3 and MurJ mainly localized at the poles (*37-40*) (**Fig. 5A**). Furthermore, our data suggests that LamA transiently and stochastically interacts with both pathways. Supporting this observation are the localizations of the likely kinase and phosphatase involved. PknA and PknB, essential kinases involved in cell growth and division, are predicted to phosphorylate LamA and localize to the poles

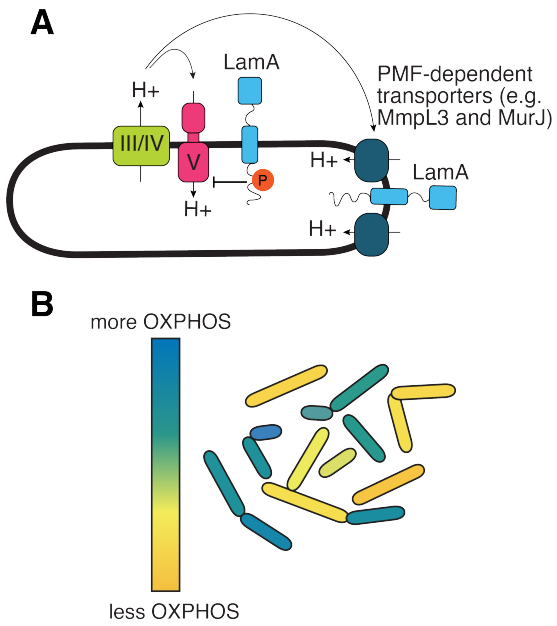

Figure 5. Model for spatial segregation and aging of metabolic processes in mycobacteria.
(A) In mycobacteria, the complexes that perform oxidative phosphorylation are physically separated from those used to grow the bacterium. Both complexes rely on the proton motive force to transport molecules across the plasma membrane. LamA dynamically interacts with both complexes and is important for coupling ATP production to growth rate in single cells. **(B)** As single mycobacterial cells age, they rely less on oxidative phosphorylation for growth. Thus, in a genetically identical population of mycobacteria cells, the flux through central metabolic pathways differs from cell to cell.

306 (*41, 42*); in contrast, the only known protein phosphatase in mycobacteria, PstP, localizes along
307 the side walls and to the septum (*43, 44*). These data suggest that LamA could be constantly in
308 motion to generate asymmetry and heterogeneity in growth and division.

309 Mycobacteria can simultaneously catabolize different carbon sources, a feature that is
310 important for the survival of pathogenic mycobacteria which rely on a mixture of fatty acids,
311 cholesterol, and carbohydrates at different points during infection (*45-47*). Our data show that the
312 metabolism of mycobacteria is even more unusual than previously recognized, as a rapidly
313 growing population can diversify its metabolism at the single-cell level (**Fig. 5B**). While *M.*
314 *tuberculosis* is thought to mainly rely on cholesterol early in infection, multiple lines of evidence
315 suggest that this species uses glycolysis at later stages of infection when the bacterial burden is
316 high (*48, 49*). Our data suggest that this may also lead to metabolic and morphological
317 heterogeneity that may be critical for the lifecycle of the pathogen. Specifically, our model
318 suggests that inhibition of multiple metabolic subpopulations may help kill mycobacterial
319 populations faster and more completely. Indeed, simultaneous inhibition of oxidative
320 phosphorylation and glycolysis leads to rapid and complete sterilization of *M. tuberculosis (50)*.
321 Thus, our data add to the growing body of evidence that understanding - and accounting for - the
322 complexity of mycobacterial physiology at the single-cell level may be the key to improving TB
323 therapy (*51-55*).

324

325 **References**

326 1. J. N. Carey *et al.*, Regulated Stochasticity in a Bacterial Signaling Network Permits
327 Tolerance to a Rapid Environmental Change. *Cell* **173**, 196-207.e114 (2018).
328 2. N. Q. Balaban, J. Merrin, R. Chait, L. Kowalik, S. Leibler, Bacterial Persistence as a
329 Phenotypic Switch. *Science* **305**, 1622-1625 (2004).
330 3. E. S. Chung, W. C. Johnson, B. B. Aldridge, Types and functions of heterogeneity in
331 mycobacteria. *Nature Reviews Microbiology* **20**, 529-541 (2022).
332 4. B. B. Aldridge *et al.*, Asymmetry and Aging of Mycobacterial Cells Lead to Variable
333 Growth and Antibiotic Susceptibility. *Science* **335**, 100-104 (2012).
334 5. E. H. Rego, R. E. Audette, E. J. Rubin, Deletion of a mycobacterial divisome factor
335 collapses single-cell phenotypic heterogeneity. *Nature* **546**, 153-157 (2017).

6. K. R. Gupta *et al.*, An essential periplasmic protein coordinates lipid trafficking and is required for asymmetric polar growth in mycobacteria. *eLife* **11**, e80395 (2022).
7. M. Campos *et al.*, A constant size extension drives bacterial cell size homeostasis. *Cell* **159**, 1433-1446 (2014).
8. J. Zeng *et al.*, Protein kinases PknA and PknB independently and coordinately regulate essential Mycobacterium tuberculosis physiologies and antimicrobial susceptibility. *PLoS Pathog* **16**, e1008452 (2020).
9. S. Fortuin *et al.*, Phosphoproteomics analysis of a clinical Mycobacterium tuberculosis Beijing isolate: expanding the mycobacterial phosphoproteome catalog. *Front Microbiol* **6**, 6 (2015).
10. K. C. Nakedi *et al.*, Identification of Novel Physiological Substrates of Mycobacterium bovis BCG Protein Kinase G (PknG) by Label-free Quantitative Phosphoproteomics. *Mol Cell Proteomics* **17**, 1365-1377 (2018).
11. S. Prisic *et al.*, Extensive phosphorylation with overlapping specificity by Mycobacterium tuberculosis serine/threonine protein kinases. *Proceedings of the National Academy of Sciences* **107**, 7521-7526 (2010).
12. R. Verma *et al.*, Quantitative Proteomic and Phosphoproteomic Analysis of H37Ra and H37Rv Strains of Mycobacterium tuberculosis. *Journal of Proteome Research* **16**, 1632-1645 (2017).
13. U. Kusebauch *et al.*, Mycobacterium tuberculosis supports protein tyrosine phosphorylation. *Proceedings of the National Academy of Sciences* **111**, 9265-9270 (2014).
14. T. Falk *et al.*, U-Net: deep learning for cell counting, detection, and morphometry. *Nature Methods* **16**, 67-70 (2019).
15. S. Berg *et al.*, ilastik: interactive machine learning for (bio)image analysis. *Nature Methods* **16**, 1226-1232 (2019).
16. K. C. Murphy. (Springer US, 2021), pp. 301-321.
17. D. J. Kiviet *et al.*, Stochasticity of metabolism and growth at the single-cell level. *Nature* **514**, 376-379 (2014).
18. M. M. Logsdon *et al.*, A Parallel Adder Coordinates Mycobacterial Cell-Cycle Progression and Cell-Size Homeostasis in the Context of Asymmetric Growth and Organization. *Current biology : CB* **27**, 3367-3374.e3367 (2017).
19. M. Priestman, P. Thomas, B. D. Robertson, V. Shahrezaei, Mycobacteria Modify Their Cell Size Control under Sub-Optimal Carbon Sources. *Front Cell Dev Biol* **5**, 64 (2017).
20. E. S. Chung, P. Kar, M. Kamkaew, A. Amir, B. B. Aldridge, Mycobacterium tuberculosis grows linearly at the single-cell level with larger variability than model organisms. *bioRxiv*, (2023).
21. J. M. Benarroch, M. Asally, The Microbiologist's Guide to Membrane Potential Dynamics. *Trends in Microbiology* **28**, 304-314 (2020).
22. J. M. Kralj, D. R. Hochbaum, A. D. Douglass, A. E. Cohen, Electrical Spiking in Escherichia coli Probed with a Fluorescent Voltage-Indicating Protein. *Science* **333**, 345-348 (2011).
23. H. Guo *et al.*, Structure of mycobacterial ATP synthase bound to the tuberculosis drug bedaquiline. *Nature* **589**, 143-147 (2021).
24. C. F. Wong *et al.*, Structural Elements Involved in ATP Hydrolysis Inhibition and ATP Synthesis of Tuberculosis and Nontuberculous Mycobacterial F-ATP Synthase Decipher New Targets for Inhibitors. *Antimicrobial Agents and Chemotherapy* **66**, e01056-01022 (2022).
25. M. G. Montgomery, J. Petri, T. E. Spikes, J. E. Walker, Structure of the ATP synthase from Mycobacterium smegmatis provides targets for treating tuberculosis. *Proceedings of the National Academy of Sciences* **118**, e2111899118 (2021).

26. H. Yaginuma *et al.*, Diversity in ATP concentrations in a single bacterial cell population revealed by quantitative single-cell imaging. *Scientific Reports* **4**, 6522 (2014).
27. S. Manuse *et al.*, Bacterial persisters are a stochastically formed subpopulation of low-energy cells. *PLOS Biology* **19**, e3001194 (2021).
28. W.-H. Lin, C. Jacobs-Wagner, Connecting single-cell ATP dynamics to overflow metabolism, cell growth, and the cell cycle in Escherichia coli. *Current Biology* **32**, 3911-3924.e3914 (2022).
29. K. Ginda *et al.*, The studies of ParA and ParB dynamics reveal asymmetry of chromosome segregation in mycobacteria. *Molecular Microbiology* **105**, 453-468 (2017).
30. M. M. Logsdon *et al.*, A Parallel Adder Coordinates Mycobacterial Cell-Cycle Progression and Cell-Size Homeostasis in the Context of Asymmetric Growth and Organization. *Current Biology* **27**, 3367-3374.e3367 (2017).
31. M. T. M. Hannebelle *et al.*, A biphasic growth model for cell pole elongation in mycobacteria. *Nature Communications* **11**, (2020).
32. Y. E. Chen *et al.*, Spatial gradient of protein phosphorylation underlies replicative asymmetry in a bacterium. *Proceedings of the National Academy of Sciences* **108**, 1052-1057 (2011).
33. M. Thanbichler, L. Shapiro, MipZ, a Spatial Regulator Coordinating Chromosome Segregation with Cell Division in Caulobacter. *Cell* **126**, 147-162 (2006).
34. S. Kretschmer, P. Schwille, Pattern formation on membranes and its role in bacterial cell division. *Current Opinion in Cell Biology* **38**, 52-59 (2016).
35. D. Kiekebusch, M. Thanbichler, Spatiotemporal organization of microbial cells by protein concentration gradients. *Trends in Microbiology* **22**, 65-73 (2014).
36. M. Christen *et al.*, Asymmetrical Distribution of the Second Messenger c-di-GMP upon Bacterial Cell Division. *Science* **328**, 1295-1297 (2010).
37. C. Carel *et al.*, Mycobacterium tuberculosis Proteins Involved in Mycolic Acid Synthesis and Transport Localize Dynamically to the Old Growing Pole and Septum. *PLoS ONE* **9**, e97148 (2014).
38. J. Zhu *et al.*, Spatiotemporal localization of proteins in mycobacteria. *Cell Reports* **37**, 110154 (2021).
39. C. L. Gee *et al.*, A Phosphorylated Pseudokinase Complex Controls Cell Wall Synthesis in Mycobacteria. *Science Signaling* **5**, ra7-ra7 (2012).
40. L. Thouvenel, J. Rech, C. Guilhot, J.-Y. Bouet, C. Chalut, In vivo imaging of MmpL transporters reveals distinct subcellular locations for export of mycolic acids and non-essential trehalose polyphleates in the mycobacterial outer membrane. *Scientific Reports* **13**, (2023).
41. M. Mir *et al.*, The extracytoplasmic domain of the Mycobacterium tuberculosis Ser/Thr kinase PknB binds specific muropeptides and is required for PknB localization. *PLoS Pathog* **7**, e1002182 (2011).
42. S. N. Nagarajan *et al.*, Protein kinase A (PknA) of Mycobacterium tuberculosis is independently activated and is critical for growth in vitro and survival of the pathogen in the host. *J Biol Chem* **290**, 9626-9645 (2015).
43. Iswahyudi *et al.*, Mycobacterial phosphatase PstP regulates global serine threonine phosphorylation and cell division. *Scientific Reports* **9**, (2019).
44. F. Shamma, E. H. Rego, C. C. Boutte, Mycobacterial serine/threonine phosphatase <scp>PstP</scp> is phosphoregulated and localized to mediate control of cell wall metabolism. *Molecular Microbiology* **118**, 47-60 (2022).
45. A. D. Baughn, K. Y. Rhee, Metabolomics of Central Carbon Metabolism in Mycobacterium tuberculosis. *Microbiology Spectrum* **2**, 10.1128/microbiolspec.mgm1122-0026-2013 (2014).

46. L. P. de Carvalho *et al.*, Metabolomics of Mycobacterium tuberculosis reveals compartmentalized co-catabolism of carbon substrates. *Chem Biol* **17**, 1122-1131 (2010).
47. Dany J. V. Beste *et al.*, 13C-Flux Spectral Analysis of Host-Pathogen Metabolism Reveals a Mixed Diet for Intracellular Mycobacterium tuberculosis. *Chemistry & Biology* **20**, 1012-1021 (2013).
48. J. Marrero, C. Trujillo, K. Y. Rhee, S. Ehrt, Glucose phosphorylation is required for Mycobacterium tuberculosis persistence in mice. *PLoS Pathog* **9**, e1003116 (2013).
49. W. Y. Phong *et al.*, Characterization of phosphofructokinase activity in Mycobacterium tuberculosis reveals that a functional glycolytic carbon flow is necessary to limit the accumulation of toxic metabolic intermediates under hypoxia. *PLoS One* **8**, e56037 (2013).
50. J. S. Mackenzie *et al.*, Bedaquiline reprograms central metabolism to reveal glycolytic vulnerability in Mycobacterium tuberculosis. *Nat Commun* **11**, 6092 (2020).
51. C. Toniolo, O. Rutschmann, J. D. McKinney, Do chance encounters between heterogeneous cells shape the outcome of tuberculosis infections? *Current Opinion in Microbiology* **59**, 72-78 (2021).
52. A. M. Cadena, S. M. Fortune, J. L. Flynn, Heterogeneity in tuberculosis. *Nature reviews.Immunology*, (2017).
53. P. L. Lin *et al.*, Sterilization of granulomas is common in active and latent tuberculosis despite within-host variability in bacterial killing. *Nature medicine* **20**, 75-79 (2014).
54. Q. Liu *et al.*, Tuberculosis treatment failure associated with evolution of antibiotic resilience. *Science* **378**, 1111-1118 (2022).
55. M. Mistretta, N. Gangneux, G. Manina, Microfluidic dose-response platform to track the dynamics of drug response in single mycobacterial cells. *Sci Rep* **12**, 19578 (2022).

464 **Acknowledgments.** We thank members of the Rego lab for thoughtful suggestions and
465 Dr. Andy Goodman for critical reading of the manuscript.
466 **Funding:** This work was supported by the Burroughs Wellcome Fund, the Searle
467 Foundation, the Pew Foundation, and National Institute of Health Grant R01AI148255 to
468 E.H.R. We also thank Yale Flow Cytometry for their assistance with BD Symphony
469 analyzer service. The Core is supported in part by an NCI Cancer Center Support Grant
470 # NIH P30 CA016359. The BD Symphony was funded by shared instrument grant # NIH
471 S10 OD026996. We also thank the MS & Proteomics Resource at Yale University for
472 providing the necessary mass spectrometers and the accompanying biotechnology tools
473 funded in part by the Yale School of Medicine and by the Office of The Director, National
474 Institutes of Health (S10OD02365101A1, S10OD019967, and S10OD018034). The
475 funders had no role in study design, data collection and analysis, decision to publish, or
476 preparation of the manuscript.
477 **Author contributions:** Conceptualization: C.M.G., K.R.G, and E.H.R. Investigation:
478 C.M.G., K.R.G, and E.H.R. Resources. C.M.G., K.R.G, Y.L., L.S., and E.H.R. Software:
479 L.S. Supervision: E.H.R. Funding acquisition: E.H.R. Writing - original draft: C.M.G.,
480 K.R.G, and E.H.R. Writing – review and editing: C.M.G., K.R.G, Y.L., L.S., and E.H.R
481 **Competing interests:** The authors declare no competing interests.
482 **Data and materials availability:** Strains developed during the study will be made
483 available from E.H.R.
484
485
486